3 Metal-to-Semiconductor Phase Transition in Vanadium-Dioxide Films

3.1 The Vanadium-Dioxide System

3.1.1 Introduction

Vanadium dioxide (VO_2) exhibits a metal-to-semiconductor first order phase transition as a function of temperature. The transition temperature is around T=340 K, as was first observed by Morin [Mor59]. The phase transition involves changes of the geometric (see Fig. 3.1) as well as electronic (see Fig. 3.2) structures. At temperatures below the transition temperature VO_2 is a semiconductor with an optical band gap E_g of ≈ 0.7 eV and with a monoclinic structure, while above the transition temperature it is a metal with a rutile or tetragonal structure.
The transition temperature close to room temperature makes VO_2 an interesting candidate for technology. The most potential application of VO_2 is as an intelligent window coating by which solar energy-transmission can be controlled automatically [Jor86]. The ability to change the transition temperature by doping [Lee86, Bur02] suggests that tungsten-doped vanadium dioxide can be used in energy-efficient windows. These smart windows or displays may find special applications in the architectural, automotive and aerospace sectors [Bab87]. Despite this strong motivation our understanding of the nature of this phase transition is still far from complete.
The phase transition manifests in a change of the electronic structure. Therefore these changes can be detected by photoemission spectroscopy. Concretely, one can directly follow changes of the density of states of the Vanadium 3d levels. As it is sketched in Fig. 3.2 at temperatures above 340 K there exists states at the Fermi level with mainly V 3d character. With decreasing temperature these states shift towards higher binding energies and a band gap opens at the Fermi level.
Thereby VO_2 changes its resistivity over several orders of magnitude [Mor59].

Our motivation to study the phase transition in VO_2 came from several studies of Cavalleri *et al.* [Cav01], using ultrafast techniques and suggesting VO_2 a good candidate for time-resolved experiments. Our goal was to photoinduce the phase

transition by laser light and to follow the changes of the electronic structure, employing synchrotron radiation.
Prior to pump-probe experiments different setups were tested to find the optimal conditions to reproduce and characterize the VO_2 phase-transition. Our systematic study started preparing different thicknesses of VO_2 thin films. We investigated the temperature of the phase transition and its relation to film preparation. In the last step of this VO_2 study described in Section 3.2.3 we tried to induce the phase transition by laser light.
The experiment has been performed using synchrotron radiation at the MBI-BESSY beamline U125/1, (Chapter 2 Section 2.2). The preparation and characterization of the films took place in an UHV system using low-energy electron diffraction (LEED), X-ray spectroscopy (XPS), and ultraviolet photoelectron spectroscopy (UPS). Two different methods to grow VO_2 films have been used. In the following sections we will explain the changes of the VO_2 valence-band edge as a function of the temperature.

3.1.2 Properties of Vanadium-Dioxide in the High and Low Temperature Phases

Above the transition temperature VO_2 is isomorphic to TiO_2, i.e. it has the rutile structure.

Metal	**Semiconductor**
tetragonal (rutile structure)	monoclinic
$a_R = b_R = 4.55$ Å	$a_m = 5.70$ Å
$c_R = 2.85$ Å	$b_m = 4.55$ Å
	$c_m = 5.37$ Å
	$\beta(a_m, c_m) = 123^o$
V-V-chain equidistant along c-Axis	V-V along c-Axis
distance: 2.85 Å	distance between the pair: 2.62 Å distance between two pairs: 3.16 Å
$1{\cdot}10^4\ \Omega^{-1}\text{cm}^{-1}$	$1{\cdot}\ 10^{-1}\ \Omega^{-1}\text{cm}^{-1}$

Table 3.1: Unit cell parameters [Zyl75] and the conductivity [Tho91, Chu92] of VO_2 in the metal and semiconductor phases.

The corresponding lattice structure is shown in Fig. 3.1a. The lattice constants for the tetragonal primitive cells are listed in Table 3.1. The vanadium atoms are embedded in an octahedral oxygen environment. The octahedra share sides along the c_R axis and thus the shortest **V-V** distance is along this direction. Below the transition temperature, the tetragonal rutile structure distorts and becomes monoclinic, isomorphic to MoO_2 (space group $P2_1 \mid c$). The size of the primitive

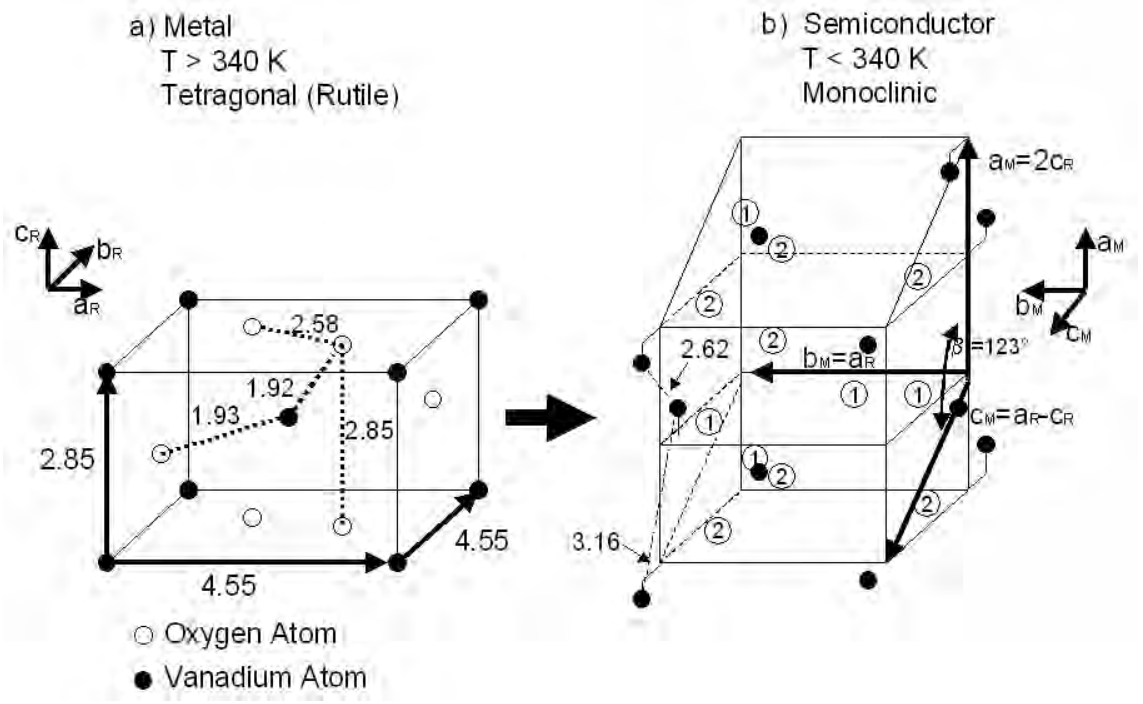

Figure 3.1: Crystal structure of VO_2. a) T > 340 K, rutile structure of the metallic phase. b) T < 340 K, monoclinic structure in the semiconducting phase and its relationship to the rutile structure. Circled 1 and 2 describe the position of the oxygen or vanadium atoms before and after the phase transition.

cell is doubled. The compact packing of the oxygen atoms remains nearly the same through out the transition. The main changes concern the vanadium atoms which are displaced from the center of the octahedra to form dimers. These geometrical changes give rise to change the optical, magnetic and transport properties (c.f. Table 3.1 and Fig. 3.3). As shown in Fig. 3.3 the transmission changes drastically in the infrared range, with higher transmission in the low temperature semiconducting phase.

3.1.3 Models Describing the Phase Transition

Several models have been proposed to describe the metal-insulator phase transition of VO_2, since it was discovered by Morin [Mor59]. The latter are Peierls-type [Goo60, Goo71, Adl67a, Adl67b, Wen94a, Wen94b] and of Mott-Hubbard-type [Mot61, Zyl75, Paq80, Ric94]. They describe lattice instabilities, electron-phonon interaction, and electron-electron correlations. Later studies proved that Cr doping of VO_2 [Mar72] leads to the formation of magnetic moments and a new phase transition in which only half of the V atoms dimerize. As this phase is also an insulator, it is suggested that the physics of VO_2 is very close to a Mott-Hubbard insula-

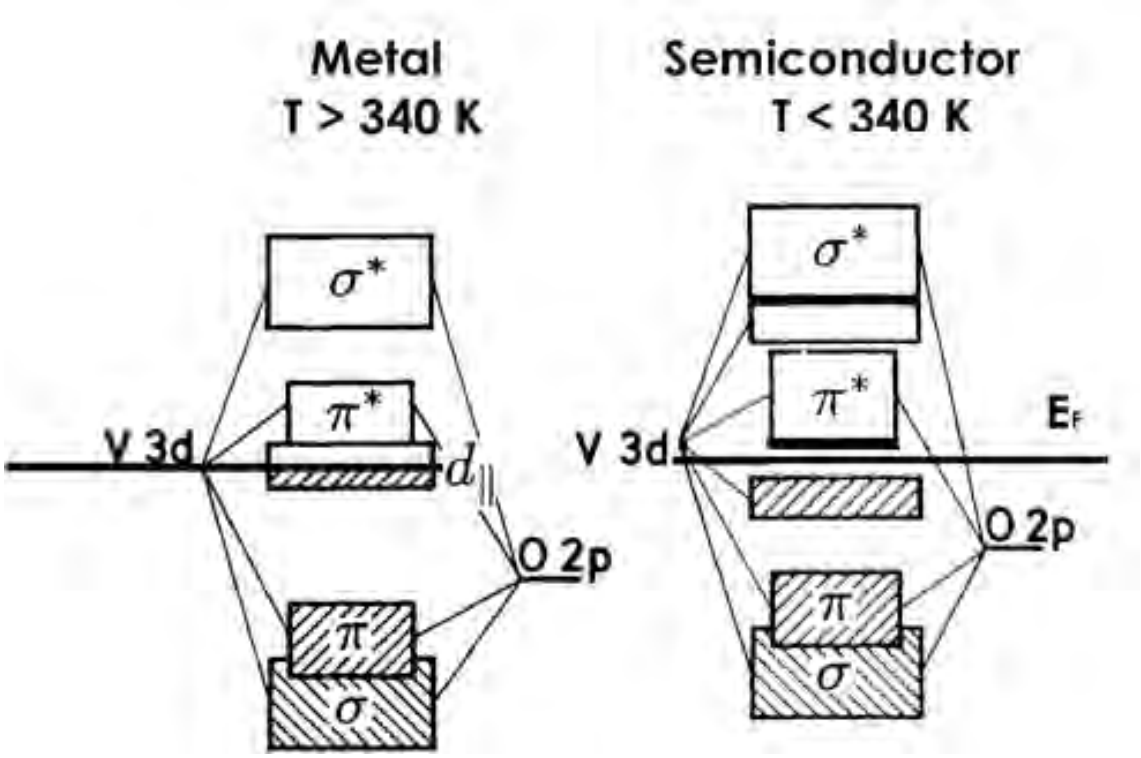

Figure 3.2: Projection of band schemes for the two VO_2 phases [Goo71, Shi90].

tor [Zyl75], which incorporates the electronic structure, the lattice distortion, and the Hubbard interaction. By thermodynamical analysis, Paquet *et al.* [Paq80] concluded that electron-electron interactions are the leading mechanism of the phase transition: the formation of V-V singlet pairs (in the insulating phase) due to a strong Coulomb correlation triggers the opening of a Peierls gap. So far, neither of these approaches has successfully explained the broad range of phenomena occurring in VO_2. Recently, Biermann *et al.* [Bie05] proposed that VO_2 behaves like a non-conventional Mott insulator, for which the formation of dynamical V-V singlet pairs due to a strong Coulomb correlation is necessary to trigger the opening of a Peierls gap.
The band scheme for both phases is illustrated in Fig. 3.2 [Goo60]. The general situation is visualized in Fig. 3.4, for the rutile phase. The O^{2-} ions (2p orbitals) stabilize the V^{4+} ions (3d orbitals) by the electrostatic Madelung energy. Figure 3.4 shows schematically the one-electron 3d, 4s, 4p energy levels for ionic V^{4+}, and the 2s, 2p energy levels for ionic O^{2-}. As illustrated in Fig. 3.1 each anion has three, coplanar nearest-neighbor cations and the anion π orbitals are directed perpendicular to this plane. The hybridization between the oxygen 2p and vanadium 3d orbitals leads to states of σ and $\sigma^\star$ as well as π and $\pi^\star$ character. While the σ- and π-states will be filled and primarily of O 2p character, the corresponding antibonding bands

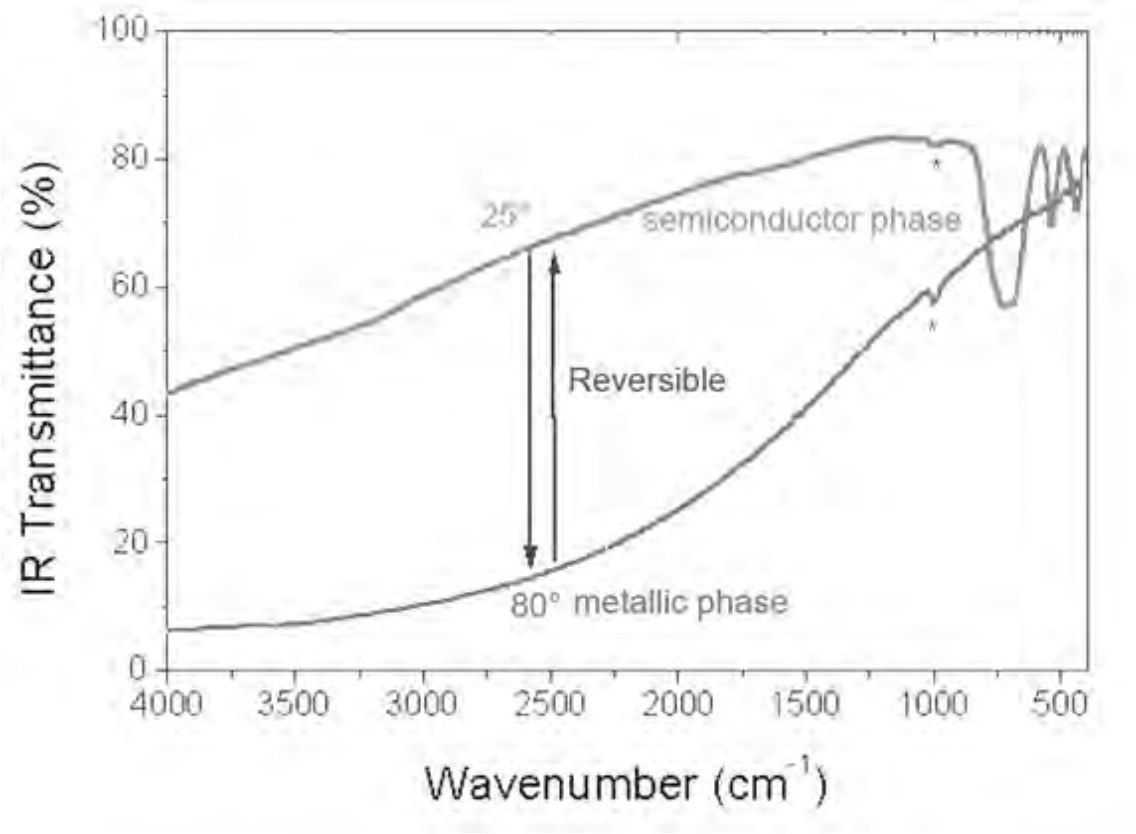

Figure 3.3: Optical transmittance below and above the transition temperature T_t=340 K of VO_2 films [Chr96].

will be dominated by the V 3d orbitals. The latter are found at and above the Fermi energy. The position and the width of the d bands are subjected not only to the p-d hybridization but also strongly influenced by direct metal-metal interactions. The d levels of the vanadium ions are split into lower lying t_{2g} states and e_g^σ states. The latter lie higher in energy and are therefore empty. The tetragonal crystal further splits the t_{2g} multiplet into an b_{1g} state and an e_g^π doublet ($d_\parallel$ and $\pi^\star$ states, respectively). The b_{1g} orbitals are oriented along the c axis (see Fig. 3.1), with σ bonding of the V-V pair in this direction.

In the monoclinic phase, the dimerization and tilting of the V-V pairs results in two important effects. First, the $b_{1g}(d_\parallel)$ band is split into a lower-energy bonding combination and a higher antibonding one, thus leaving the $d_\parallel$ band half-filled. Second, the V_d-O_p antibonding e_g^π states are pushed higher in energy, due to the tilting of the pairs which increases the overlap of these states with O derived states. The single electron occupies the $d_\parallel$-bonding combination, resulting in a Peierls-like band gap.

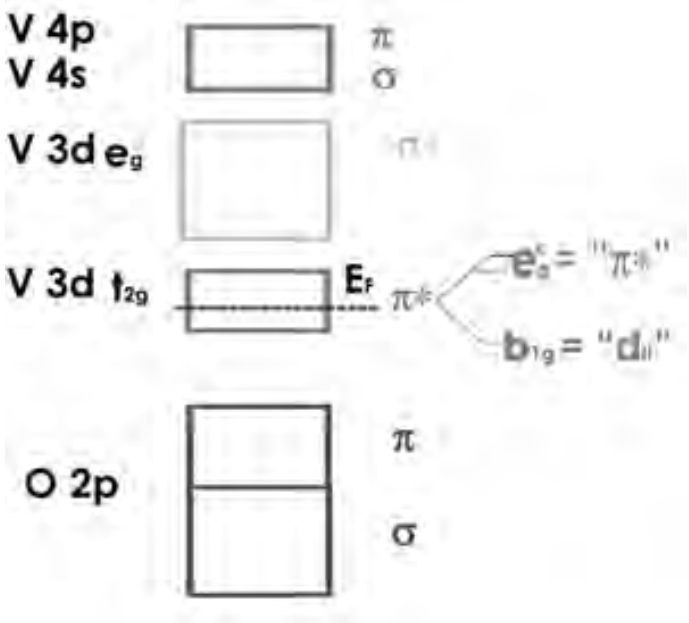

Figure 3.4: Molecular orbital scheme for rutile VO_2.

3.2 Characterization of Vanadium-Dioxide Films

This section describes two different methods to grow VO_2. The first method is epitaxial growth of VO_2 on TiO_2(110) and has been applied for thin films (Section 3.2.1). The second method is growth of VO_2 by reactive radio-frequency sputtering (Section 3.2.2). For both methods, films were characterized by low-energy electron diffraction (LEED), atomic force microscopy (AFM), and photoemission spectroscopy of valence band and core level.

3.2.1 VO_2 grown on TiO_2(110)

In order to study the phase transition for VO_2-films high-quality crystals are required. Since VO_2 single crystals are extremely difficult to grow, we decided to grow VO_2-films on TiO_2(110). Varying the film thickness allows to investigate the influence of the interface between the TiO_2 substrate and the VO_2 film.
The most important reason for choosing TiO_2 as substrate is that rutile TiO_2 (E_g = 3.1 eV) has a larger band gap than VO_2 (E_g = 0.7 eV). This assures no superposition of VO_2 and TiO_2 valence band peaks in photoemission. Furthermore, TiO_2 has the same geometric structure (rutile) as VO_2 at temperatures above the transition temperature, a prerequisite for epitaxial growth. Other reasons are the particular stability of the TiO_2 cleaned surface, relatively low cost of good-quality commercial single-crystals, and the existence of well-known simple and reproducible

procedures for preparing high-quality surfaces under UHV conditions. Cleaned VO_2 surfaces have sufficient bulk-oxygen vacancies, which suppress charging effects and exhibit a simple and well-known electronic structure typical for closed-shell oxides [Die03].

Ultrathin VO_2 Films on TiO_2

Substrate Preparation Sample preparation was performed in an UHV chamber operating at a base pressure of $5 \cdot 10^{-11}$ mbar. The $TiO_2(110)$ crystal was cleaned by cycles of Ar-ion sputtering at 500 V, followed by annealing to 900-1000 K. The cleaning cycles were repeated until a sharp (1×1) LEED pattern was observed.

Film Deposition The VO_2 coverage has been by vanadium deposition and oxidation on TiO_2. Oxidation was carried out at 10^{-8} mbar partial pressure of oxygen while annealing the sample to about 470 K. VO_2 films with a thickness of up to 8 monolayers (ML) were growth on TiO_2. A monolayer of VO_2 corresponds to a thickness of about 2.62 Å.

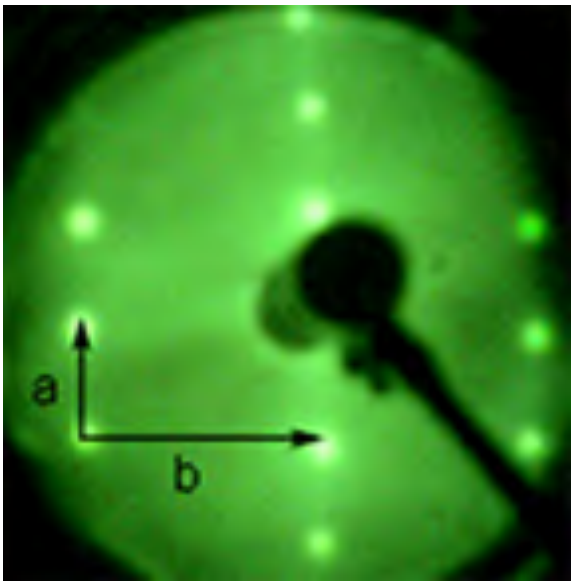

Figure 3.5: LEED diffraction-pattern of 3ML of VO_2 on $TiO_2(110)$ recorded at an electron energy of 120 eV .

Characterization by LEED Figure 3.5 shows the LEED pattern of 3 ML VO_2 on $TiO_2(110)$. The periodicity of the pattern resembles that of the clean surface but

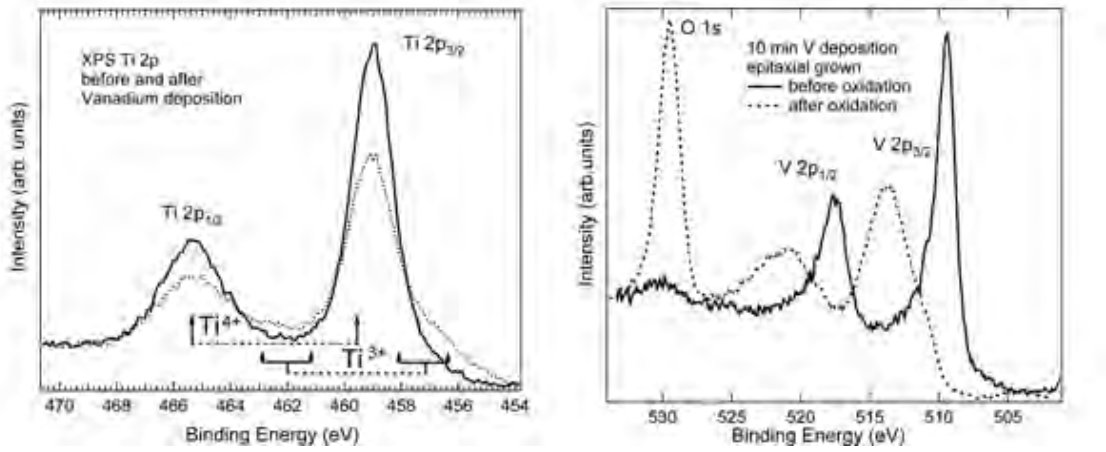

Figure 3.6: Core level spectra characterizing the growth of VO_2 on the TiO_2 substrate. a) The Ti 2p core-level before (full lines) and after (dotted lines) vanadium deposition. b) The V 2p core-level before oxidation (full lines) and after oxidation by an exposure of $600 \cdot 10^{-8}$ mbar $\cdot$ s and annealing to 413 K (dotted lines).

the spots are less sharp [Sam96]. This indicates an epitaxial growth of vanadium dioxide on the $TiO_2(110)$ surface. After subsequent deposition of vanadium and oxidation, the LEED pattern becomes faint and hardly detectable. For this reason was annealed to 470 K during or after the sample oxidation. This improves the surface order and likely reoxidizes the Ti surface atoms which become reduced by the deposited Vanadium. After annealing, a reasonably sharp (1×1) LEED pattern was recovered, as shown in Fig. 3.5.

Characterization of Stoichiometry and Coverage by XPS By comparison with previous studies XPS allows to identify the oxidation state of the vanadium-oxide films. Furthermore, XPS is used to calibrate the coverage of the thin films. Figure 3.6a shows XP-spectra of the Ti and V 2p levels before and after V deposition as well as oxidation. The binding energy scale refers to the Fermi level of the sample by assuming an analyzer work function of 4.4 eV. The Ti 2p core levels are a very good sensor for the stoichiometry of TiO_2 surfaces. Lower oxidation stages of titanium appear as shoulders at the lower binding energy side and indicate a reduction of the substrate when metallic vanadium is deposited. According to Diebold *et al.* [Die03] deposition of vanadium in an oxygen ambience results in vanadium oxide, that interacts with the substrate because the deposition of Vanadium reduces the TiO_2 surface [Bie99]. Surface reduction is confirmed by Ti 2p XPS spectra, shown in Fig. 3.6. The solid curve in Fig. 3.6a is the Ti 2p core-level spectrum of the stoichiometric TiO_2 and clean surface, where only Ti^{4+} cations are present. The main effect of V deposition on the Ti 2p XP-spectrum is the appearance of shoulders on

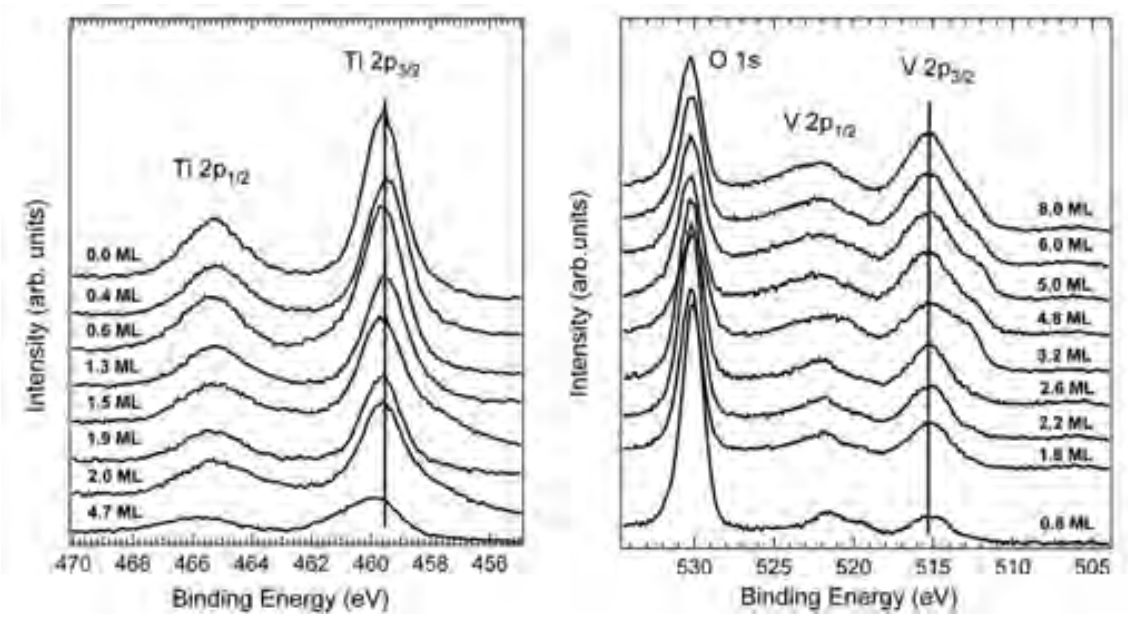

Figure 3.7: XP-spectra of the Ti 2p (a) and V 2p and O 1s (b) core levels for increasing thickness of vanadium oxide on $TiO_2(110)$. The photon energy was 1253.6 eV, i.e., $K_{\alpha 1,2}$ radiation from a Mg anode. For coverage calibration see text.

the low -binding-energy side of the Ti^{4+} 2p XP-peaks, which arise from the presence of Ti^{3+} ions (dashed line in Fig. 3.6). Two binding energies are indicated for each of the spin-orbit split Ti^{3+} 2p core levels since the XP-spectrum for Ti^{3+} ions exhibits multiple peaks due to final-state screening effects [Zha92]. The broadening of the Ti 2p core-level spectrum may indicate an electron transfer from the reactive overlayer to the substrate Ti ions. Another possibility could be oxygen is physically extracted from the TiO_2 surface and incorporated into the overlayer [Die03].
Figure 3.6b shows photoemission spectra of the V 2p core-level after 6 ML of vanadium deposition on TiO_2 crystal, before (solid lines) and after (dashed lines) oxidation for an exposure of $600 \cdot 10^{-8}$ mbar $\cdot$ s and at a sample temperature of 410 K. After oxidation the V $2p_{1/2}$ and V $2p_{3/2}$ photoemission lines are broader as the corresponding metallic Vanadium peaks. Furthermore, the intensity of the vanadium core-levels decreases by about a factor of two upon oxidation. The broadening due to many different oxidation stages is pronounced for the d-elements, which exhibit small linewidths [Saw79] in the metallic phase.

In order to characterize the stoichiometry of the VO_2 films Ti 2p, V 2p and O 1s XP-spectra were measured for increasing VO_2 film thickness. Results are summarized in Fig. 3.7. Figure 3.7a shows core-level spectra of the Ti 2p level for increasing Vanadium coverage. The background due to secondary electrons [Shi72] has been subtracted in every spectrum. The Ti $2p_{3/2}$ emission line is found at a

binding energy of 459 eV for the clean, stoichiometric surface. For coverages above 4 ML it exhibits a binding energy shift of 0.6 eV in agreement with the findings in reference [Sam97]. The Ti $2p_{1/2}$ component is separated by 6.2 eV from the Ti $2p_{3/2}$ component and shows a comparable behavior. The Ti 2p spectra have been fitted with three Gaussian functions and has been subtracted a Shirley background, as shown in Fig. 3.8a. The analysis of the width of the Ti 2p lines reveals a broadening of both peaks with increasing VO_2 film thickness, as listed in Table 3.2.

In Fig. 3.7b three features can be distinguished. The first two peaks at lower

Coverage [ML]	FWHM($V2p_{3/2}$) [eV]	FWHM($V2p_{1/2}$) [eV]	I(A) [arb.units]
1	2.30(2)	3.12(5)	0.0055(2)
2.60	2.35	3.33(8)	0.064(1)
5.0	2.41(2)	3.42(3)	0.23(10)
6.0	2.44(3)	3.50(10)	0.24(10)

Table 3.2: Results of the analysis of the V 2p core-level spectra for increasing VO_2 coverage on TiO_2.

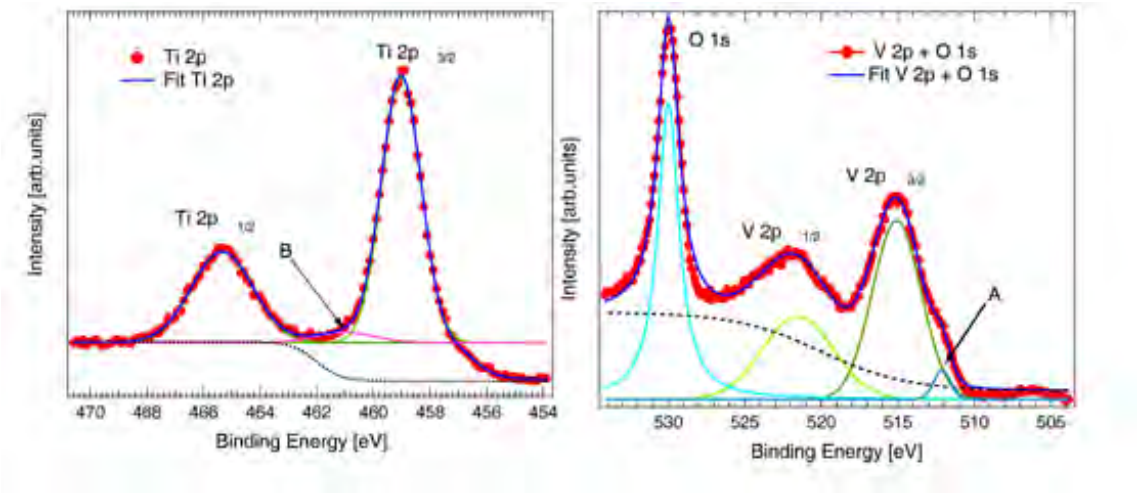

Figure 3.8: a) Ti 2p core-level spectrum (doted lines) and fit function (solid lines). b) V 2p plus O 1s core-level spectra (doted lines) and fit function (solid lines).

binding energy correspond to the V $2p_{1/2}$ and V $2p_{3/2}$ emission lines, while the third peak at higher binding energy originates from the O 1s core-level. The position of the O1s peak for vanadium oxides depends only weakly on the vanadium oxidation stage as discussed in Refs. [Tep02, Saw79, Zha94]. More sensitive to the stoichiometry of the vanadium oxide are the changes of the V 2p spectra. The overall shape of the spectra [Men95] and in particular the FWHM (Full Width at Half Maximum)

significantly differs for different oxides of vanadium as it is discussed in [Men95]. Evidently, our thin films can not be V_2O_5. The fits in Fig. 3.8 reveal another feature to be discussed Peak **A** in the vicinity of the V $2p_{3/2}$ line at about 512.25 eV. This peak could stem from a different oxide. The amplitude of the peak increases for increasing coverage as summarized in Table 3.2. Likewise, the V 2p lines broaden when the coverage is increased. We conclude that the V 2p emission lines inhomogeneously broaden upon deposition and that the XP-spectra exhibit mainly VO_2 character.

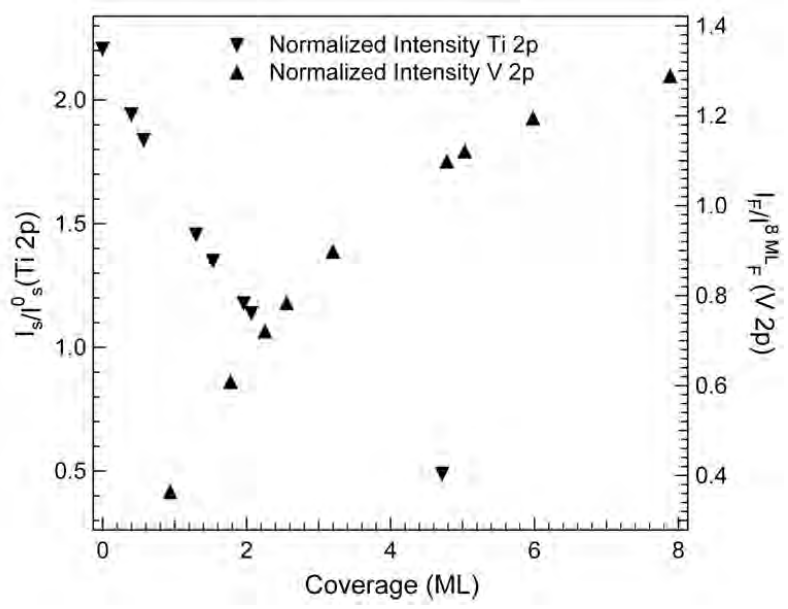

Figure 3.9: Normalized core-level intensities of the Ti $2p_{3/2}$ substrate-peak and V $2p_{3/2}$ overlayer-peak as a function of coverage.

Film thickness have been calibrated by XPS measurements [Fad84]. The intensity I of the observed core level signal depends on the mean-free path of electrons λ. The photocurrent dI, originating from a layer of thickness dz, at a depth z, detected at an angle θ with respect to the surface normal is given by:

$$dI \propto e^{-\frac{z}{\lambda \cos\theta}} \tag{3.1}$$

The intensity of the photoemission signal of the substrate I_S is monitored as a function of the thickness of the overlayer F. The effective attenuation length is obtained from the electron current from the overlayer signal I_F, assuming identical attenuation length for film and substrate. The thickness of the film is calculated for normal detection ($\cos\theta = 1$) to:

$$\frac{I^F}{I^F_{8ML}} = 1 - e^{\frac{-t}{\lambda}} \tag{3.2}$$

where I^F_{8ML} is the intensity measured for bulk VO_2, and t is the number of monolayer deposited. The intensity originating from substrate atoms after deposition of t monolayers of the film is given by:

$$\frac{I^S}{I^S_0} = e^{\frac{-t}{\lambda}} \tag{3.3}$$

where I^S_0 is the intensity of the substrate core-level without any deposited film. For excitation with a photon energy of 1253 eV and a Ti 2p binding energy of 490 eV a kinetic energy of the photoemitted electrons of about 600 eV results. This corresponds to an escape depth of $\lambda \approx 10$ Å according to the universal curve of inelastic mean-free path in Chapter 2 Section 2.1. The vertical interlayer distance between two successive cation planes (c=3.22 Å see Table 3.1) is here defined as the thickness of 1 ML of VO_2.

In Fig. 3.7a we see that the height of the Ti 2p photoemission peak decreases when the thickness of the VO_2 layer increases. Figure 3.9 summarizes the intensity ratios as a function of the coverage, calculated by Eq. 3.2 and 3.3.

Characterization of the Valence Electronic Structure by UPS Figure 3.10 shows the valence-band structure for 3 ML thin VO_2-films. The V 3d band is located at 1.78 eV binding energy and the O 2p-band exhibits two components at 5.5 eV and 8 eV, with an overall width of 4.5 eV. These data are in accordance with the results from Negra *et al.* [Neg01]. The angle-resolved photoemission spectra reveal a significant dispersion along the [001] direction for the O 2p valence band at approximately 4 eV binding energy while for the V 3d level no dispersion is observable. The O 2p orbital has a significant delocalized character as compared to the localized V 3d orbital suggesting negligible hybridization between O 2p and V 3d. Figure 3.11 shows valence-band photoemission spectra for different VO_2 film thicknesses on TiO_2. Spectra have been recorded at a photon energy of 21.2 eV, using a discharge helium lamp. The shape of the V 3d peak changes drastically with increasing thickness. This indicates a strong interaction between the deposited vanadium and the TiO_2 surface at the early stage of growth, i.e, submonolayer coverage. Up to 0.8 ML of VO_2 on TiO_2, the V 3d region displays a small density of states close to the Fermi level. The shift of the V 3d edge and also the changes of its shape are better observable in Fig. 3.11b. The intensity of the V 3d peak increases up to a film thickness of 3 ML and saturates for higher coverage. The V 3d edge shifts to higher binding energy for increasing coverage. The oxygen component lies in the range from 3 eV to 10 eV binding energy and exhibits VO_2 typical features [Shi90]. It shows no remarkable change with respect to the coverage.

Phase Transition Figure 3.12 shows three photoemission spectra of the VO_2 valence band. Spectra have been recorded for temperatures of 387 K, 300 K, and 138

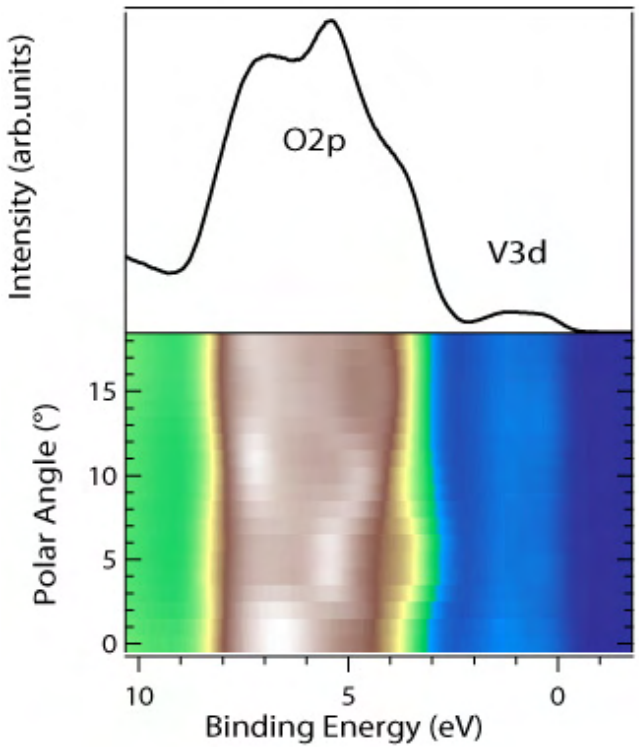

Figure 3.10: Angle-resolved photoemission spectra showing of the VO_2 valence band for 3 ML VO_2 on $TiO_2(110)$. Spectra are recorded along the [001] direction for emission angles of 0^o to 15^o.

K. Annealing and cooling rates were 1.6 K/min and 2.7 K/min. For temperatures below and above the phase transition temperature of 340 K, we expect an energetic shift of the valence-band edge $\Delta E = E_{Edge}$ and a change of its shape.

However, only in the V 3d region a small change of the shape of the photoemission spectra with temperature is observed. The shift of the V 3d region is 33 meV at 387 K. This shift of the valence band is negligible compared to the expected shift of the V3d region due to a gap opening provoked by the metal to semiconductor phase-transition.
We have to conclude that the phase transition is not observed for ultrathin films. This is attributed to the strong interaction between the VO_2 films and the TiO_2 substrate. Furthermore, we notice that temperature-induced broadening of the spectra is negligible.

100 nm Thick VO_2 Film

To minimize the influence of substrate. VO_2 films with a larger thickness have been grown on $TiO_2(110)$ by vanadium deposition in an oxygen atmosphere of $p_o = 10^{-6}$

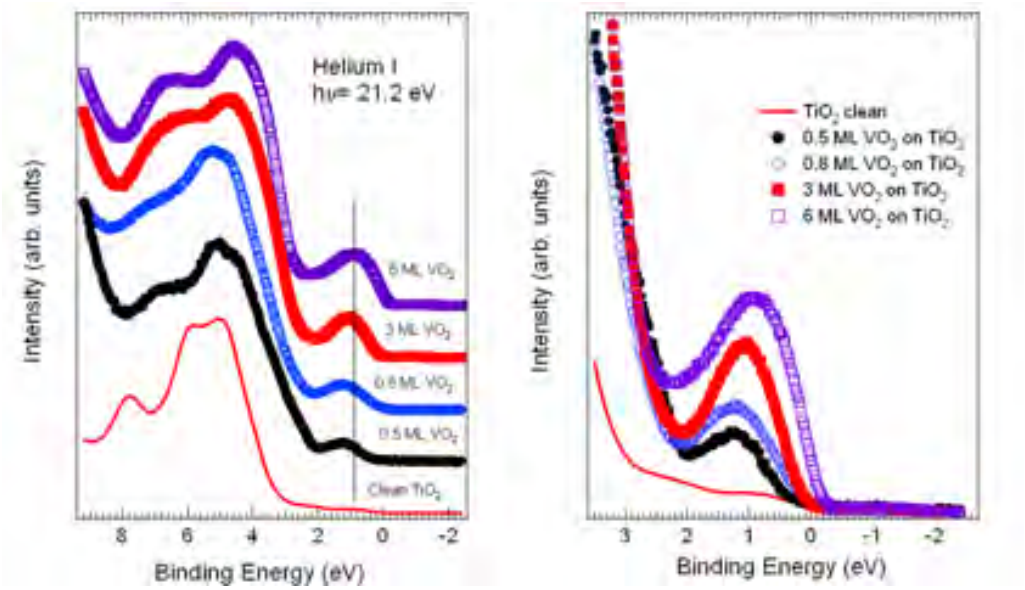

Figure 3.11: Valence band photoemission spectra of ultrathin VO_2 layers grown on the TiO_2 surface. a) He I valence band spectra at a photon energy of $h\nu = 21.2$ eV. b) Zoom of the V3d region. All spectra were measured at room temperature and for normal emission.

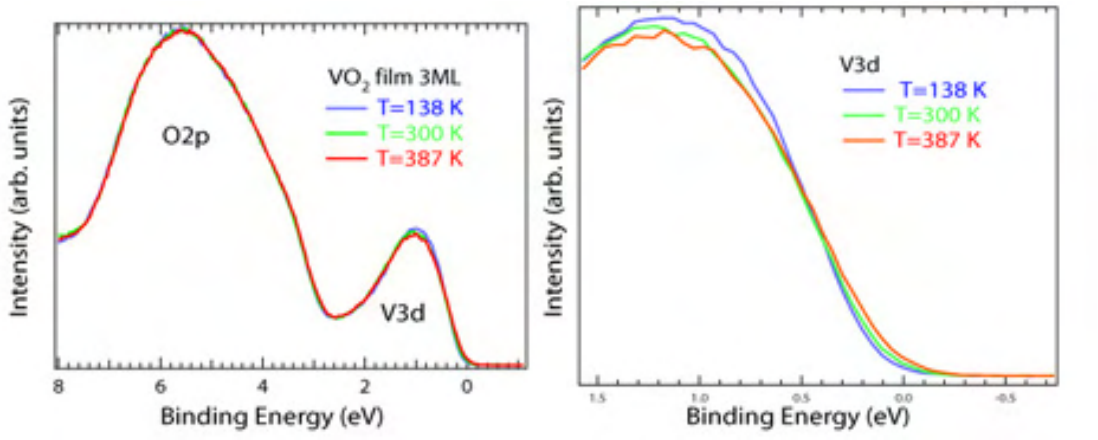

Figure 3.12: Valence-band photoemission spectra of 3 ML VO_2 film on TiO_2. a) Valence band photoemission spectra at 387 K, 138 K and room temperature, for normal emission. b) Zoom of the V3d region.

mbar. The temperature of the $TiO_2(110)$ sample during the deposition process was approximately 700 K. Figure 3.13a shows a LEED pattern of 100 nm thick VO_2-

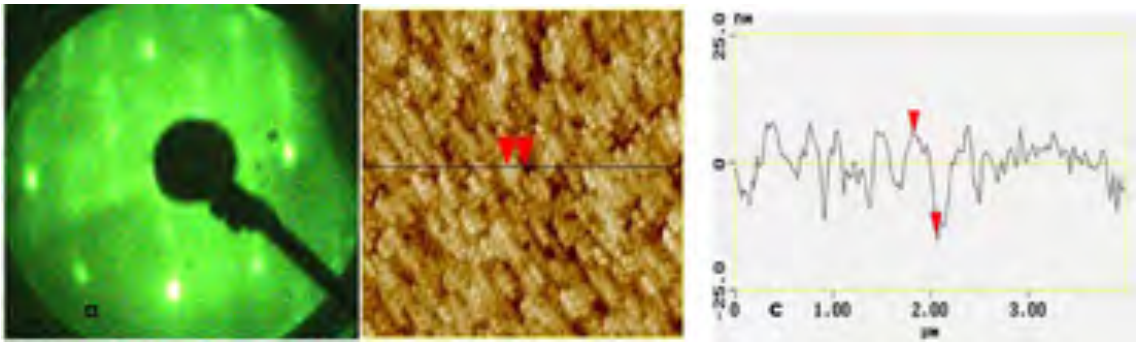

Figure 3.13: 100 nm thick VO_2 film on $TiO_2(110)$. The film is grown by evaporation of vanadium in an O_2-atmosphere. a) LEED pattern recorded at 92 eV is characteristic for a polycrystalline structure. b) Ex-situ AFM-picture ($4x4\mu m^2$) shows preferential azimuthal orientation. c) The line profile taken along the black line in the middle figure shows a vertical corrugation of approximately 13 nm.

films on $TiO_2(110)$. The LEED pattern reveals a polycrystalline structure, namely a large number of single crystals with preferential azimuthal orientation along the high symmetry direction of the underlying substrate.
Atomic force micrographs have been taken, see Fig. 3.13b, which show the morphology of these thick films. The vertical profile of the surface is plotted in Fig. 3.13c. The preferential azimuthal orientation of the crystallites is also visible in the AFM picture.
As already discussed, for the transition from a semiconducting, low-temperature phase into a metallic, high-temperature phase a closing of the electronic band gap is expected. This should manifest in a shift of the valence-band edge towards lower binding energies, which may be accompanied by a change of the shape of the edge. Valence-band photoemission spectra have been taken for different temperatures. Figure 3.14 shows again the V 3d region for 123 K, 300 K, and 371 K. The changes of the shape of the photoemission spectra at different temperatures for 100 nm thick films are more apparent than for the ultrathin films discussed in Section 3.2.1. The heating rate was 1.40 K/min and the cooling rate was 5.60 K/min. However, even for the 100 nm thick films a semiconductor to metal phase-transition is not observed.

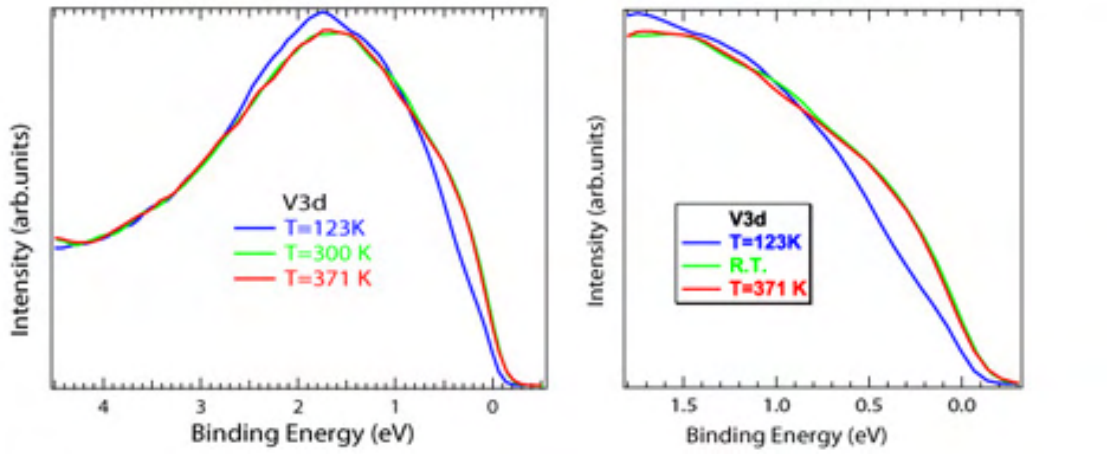

Figure 3.14: 100 nm thick VO_2 film on TiO_2(110). a) Photoemission spectra of the V3d region for three different temperatures recorded for a photon energy of 60 eV. b) Zoom in normal emission.

3.2.2 VO_2 grown by Reactive RF Sputtering.

We concluded in the last section that VO_2 films grown on TiO_2 show only small changes in the region of the valence band edge as a function of temperature. This is in contrast to VO_2 films on glass (SiO_2) prepared by reactive radio-frequency sputtering deposition. These films have been prepared by A. Polity in the group of experimental physics at the University of Gießen. The films show reversible changes of the transmission, which are interpreted in terms of a Semiconductor-to-Metal phase transition. Figure 3.15 shows the transmission at a photon energy of 0.62 eV (2000 nm). The transmission of the VO_2 films changes by 50 % for a temperature variation of 20 °C.

Characterization by AFM Figure 3.16a shows an AFM-picture in which crystallites of different size. The VO_2 films do not show any preferential orientation on the substrate as compared to the AFM-pattern, for VO_2 thin films on TiO_2 (see Fig. 3.13). The VO_2 on glass has present an overall roughness of 100 nm and is composed of large crystallites.

Characterization by XPS In order to verify that these amorphous films are indeed VO_2, core level spectra of VO_2 grown on TiO_2 and of VO_2 grown on glass are compared in Fig. 3.17. Besides a small shift the spectra are nearly seemingly identical. This proves that both samples have identical VO_2 stoichiometry.

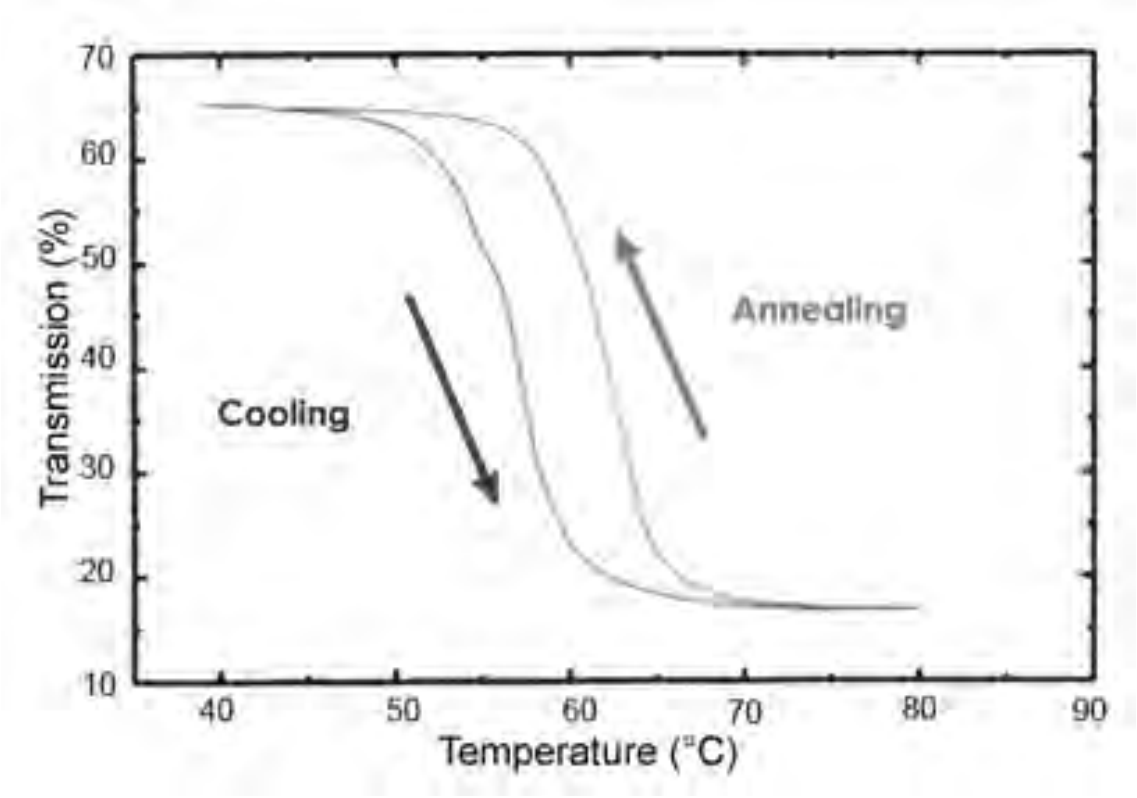

Figure 3.15: 200 nm VO_2 on glass float, transmission recorded at a wavelength of $\lambda =$ 2000 nm as a function of temperature.

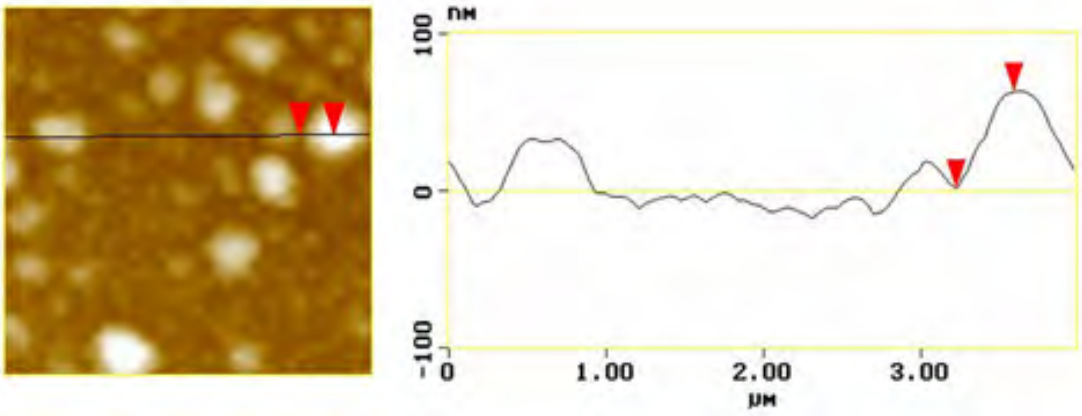

Figure 3.16: Characterization of a 200 nm VO_2 thick film on float glass, prepared by radio frequency sputtering. a) Ex-situ AFM-picture (4x4 μm^2) along the black line. b) The profile shows height corrugation of approximately 62 nm.

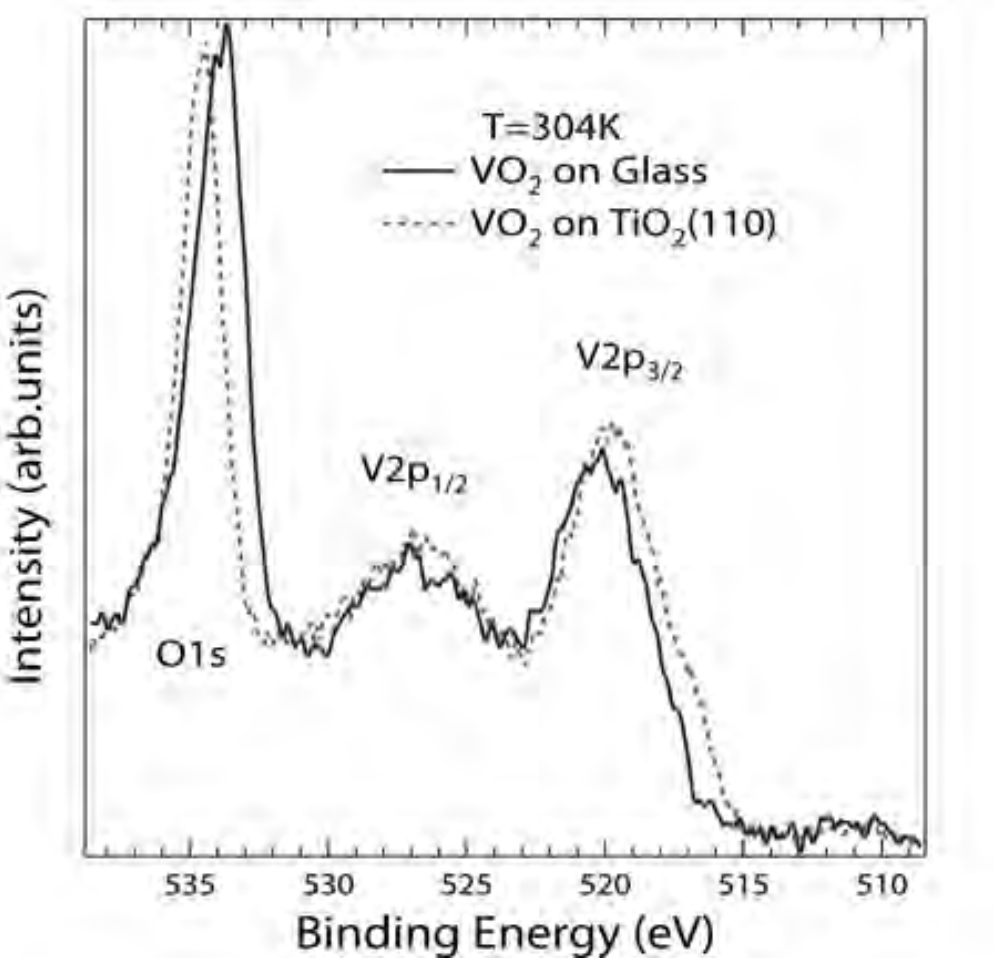

Figure 3.17: O1s and V2p core-level spectra. The solid spectrum correspond to a VO_2 film on glass grown by reactive radio frequency sputtering. The doted spectrum correspond to a 100 nm VO_2 film grown on TiO_2. Both spectra represent the same stoichiometric. Photon energy was 1253.6 eV, K_α radiation from a Mg anode.

Phase Transition Prior to the photoemission experiments, the VO_2 film on glass was annealed to 680 K to desorb possible contaminants. Figure 3.18 shows photoemission spectra in the range of the V3d valence band for different temperatures recorded at $h\nu = 60\ eV$ for normal emission. The position of the Fermi level is determined by a gold sample and is found at a kinetic energy of =53.3 eV. Upon annealing, a shift of the valence band edge and a change of the shape of the whole V 3d region is observable. They changes are interpreted as a change of the density of states in the V3d region close to the Fermi level and attributed to the closing of the semiconductor gap a Semiconductor-to-Metal Phase Transition. Note that the observed changes of the electronic structure have to occur in the few topmost layers as the surface near region is probed by UPS.

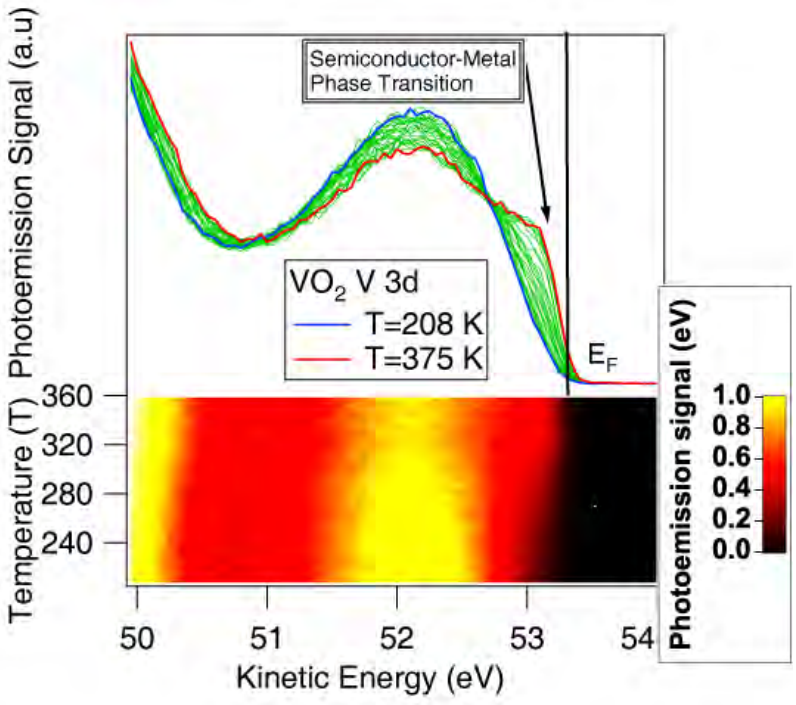

Figure 3.18: Top panel: Photoemission spectra recorded at $h\nu = 60\ eV$ and different substrate temperature for a 200 nm thick VO_2-film grown by reactive radio-frequency sputtering. Bottom panel: The same set of spectra shown in a 2D plot.

Influence of Sample Treatment In Fig. 3.19 the V 3d valence band is depicted for two different sample treatments. The first treatment consists in an one-time annealing to 600 K. Afterwards several photoemission spectra at different temperatures ranging from 199 K to 365 K were taken. The spectrum recorded at 199 K does not show V 3d density of states up to the Fermi level, which is the typical behavior for a semiconductor. As the sample temperature increases above the transition temperature, the valence edge shifts towards lower binding energy. The spectrum recorded at 365 K shows a substantial enlargement of the density of states close to the Fermi level, which is characteristic for metallic behavior. We therefore conclude that a temperature-induced metal-to-semiconductor phase transition takes place.

The second treatment consisted of several annealing cycles for the same sample up to 650 K. Figure 3.19b shows the V3d region after annealing the sample for three times to 600 K. After repetitive annealing, the metallic component is lost, since no states exist at and across the Fermi level. Now a semiconductor-to-semiconductor phase transition takes place. The nature of the phase transition depends on the

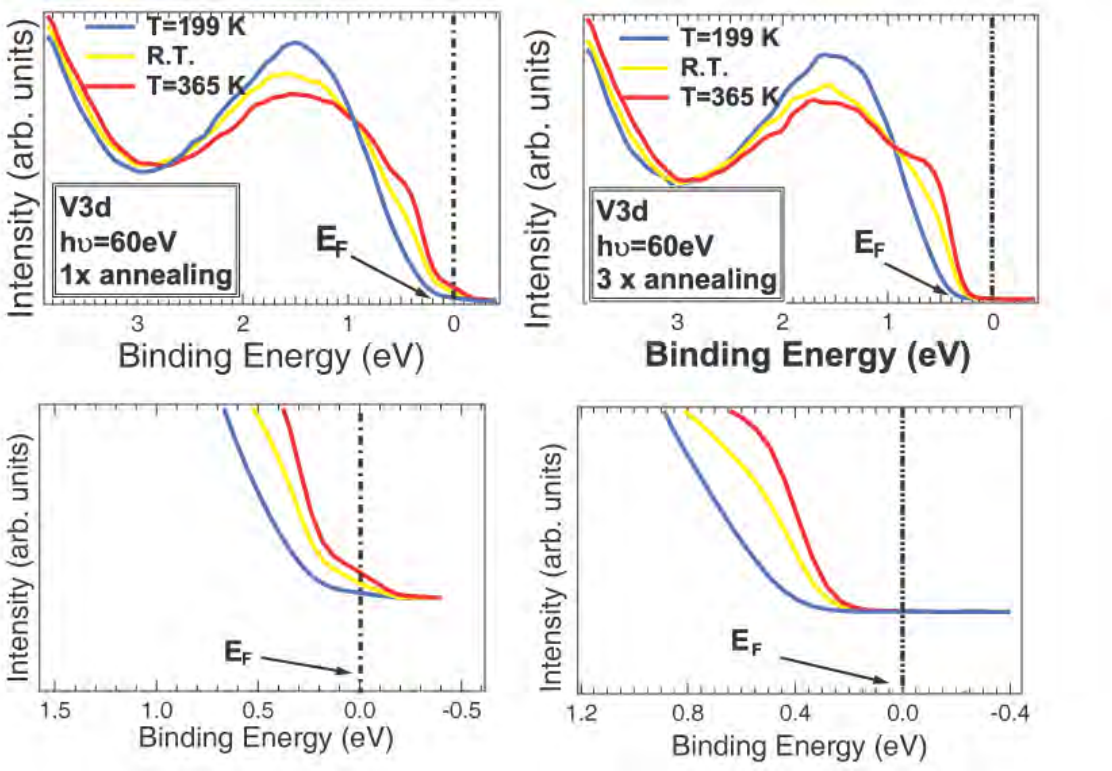

Figure 3.19: Photoemission spectra of the V3d valence band at 199 K, 300 K, and 356 K. Top,a: **Semiconductor-to-Metal Phase Transition**. Photoemission spectra after one time annealing to 600 K, **first preparation** Top, b: **Semiconductor-to-Semiconductor Phase Transition**. Photoemission spectra for the same sample after three times annealing the sample to 600 K, **second preparation**. Below: Zoom into the Fermi level region for both preparations.

sample treatment. Upon repetitive annealing of the sample in UHV, the probability to create vacancies on the surface in terms of a loss of oxygen is extremely high. Both transitions represent distinct changes of the shape of the valence band edge for temperatures above and below the transition temperature as compared to the small changes seen for VO_2 films on TiO_2.

Analysis of V 3d Spectra In order to quantify the results, the V3d region was fitted by 6 arbitrary chosen Gaussian functions. To follow the change with temperature the only parameter left variable was the amplitude of the Gaussians:

$$I_{V3d}(E,T) = bgr + \sum_{i=1}^{6} A_i(T) e^{-[\frac{E-E_F-E_p}{\sigma}]^2} \tag{3.4}$$

with *bgr* the background function, $A_i(T)$ the amplitude of the gauss components, which depend on the temperature, E_F the Fermi level position, E_p the position of each gaussian peak and σ the gaussian broadening.

Figure 3.20b displays the different amplitudes $A_i(T)$ versus temperature between 199 K to 365 K. For the first preparation (see Fig. 3.20b) every amplitude shows the same temperature dependence. The amplitude components A_5 and A_6 were used to define the temperature of the phase transition by calculating the second derivative of 300 ± 4 K.

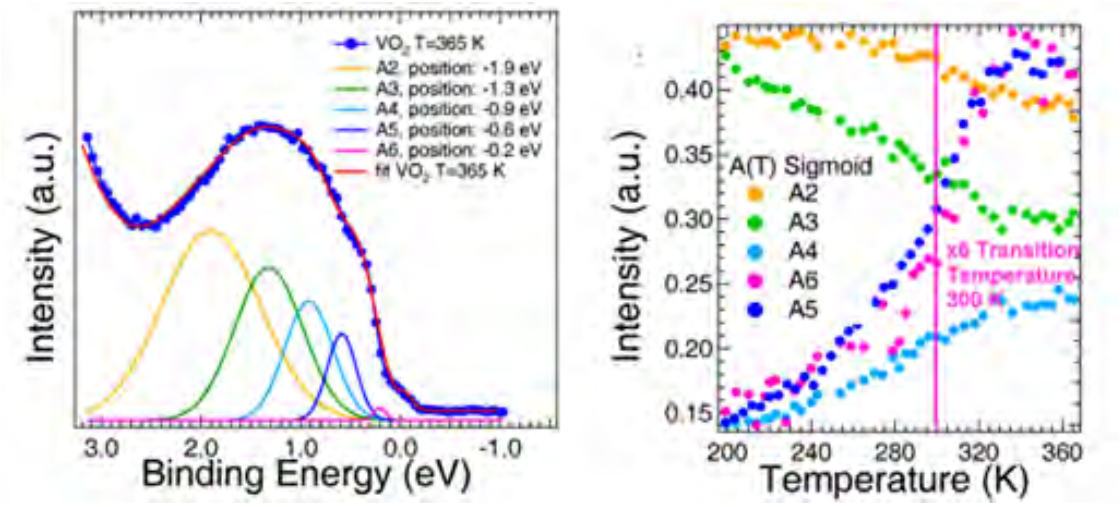

Figure 3.20: Spectral decomposition of photoemission spectra in a temperature range between 265 K and 360 K. a) The Metal-to-Semiconductor Phase Transition, 200 nm thick VO_2 film at a temperature of T=360 K. b) Temperature dependence of the different Gaussian amplitudes.

To fit the spectra obtained for the second preparation the amplitude component A_6, which represents the metallic component was omitted. Following the same data evaluation the transition temperature is determined to 220 ± 4 K.

A research group at the University of Giessen has demonstrated that the transition temperature is lower, when the doping of the VO_2 films with Fluorine and Tungsten is increased. Such a decrease of the transition temperature by atomic substitutions is known since B. Goodenough [Goo71].
In contrast to the group in Giessen, which is measuring bulk properties, the experimental techniques used here are surface sensitive. The transition temperature of the second preparation, of 220 K is lower when compared to the transition temperature of the first preparation of 300 K. This could be explained by an increase of defects upon repeated annealing of the sample and concomitant changes of the stoichiometry.
In order to check whether the phase transition is reversible, photoemission spectra

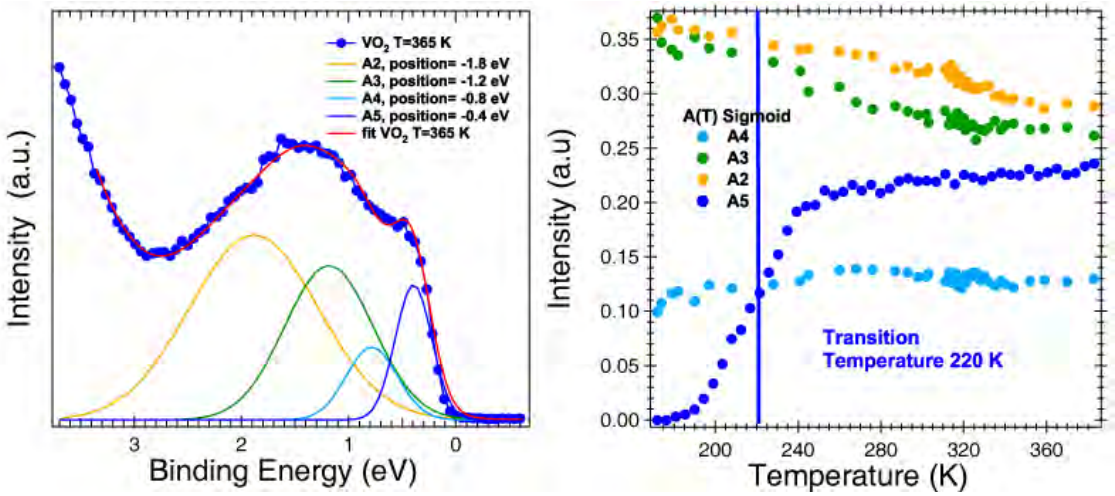

Figure 3.21: Spectral decomposition of photoemission spectra in a temperature range between 200 K and 365 K. a) Photoemission spectrum for a 200 nm thick VO_2 film at a temperature of T=360 K and the fit functions used. b) Temperature dependence of the different Gaussian amplitudes.

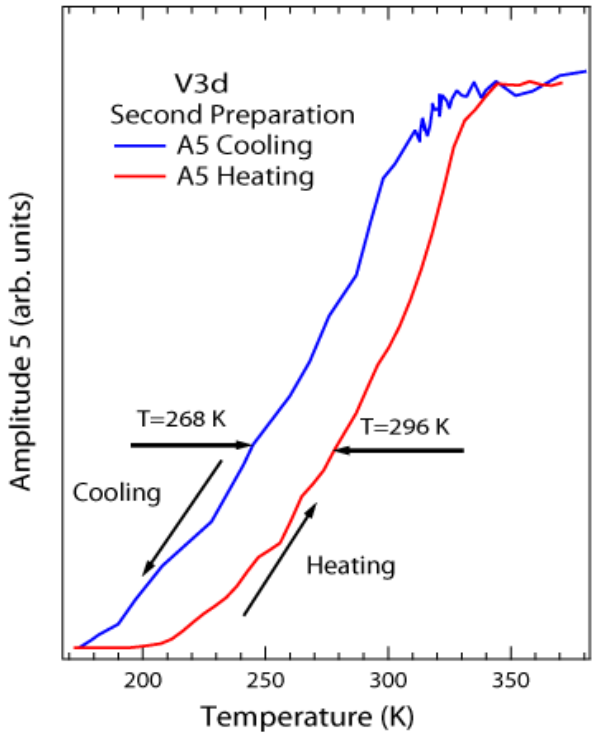

Figure 3.22: Hysteresis loop for the semiconductor-to-semiconductor phase transition. Depicted is the amplitude A_5 as a function of temperature.

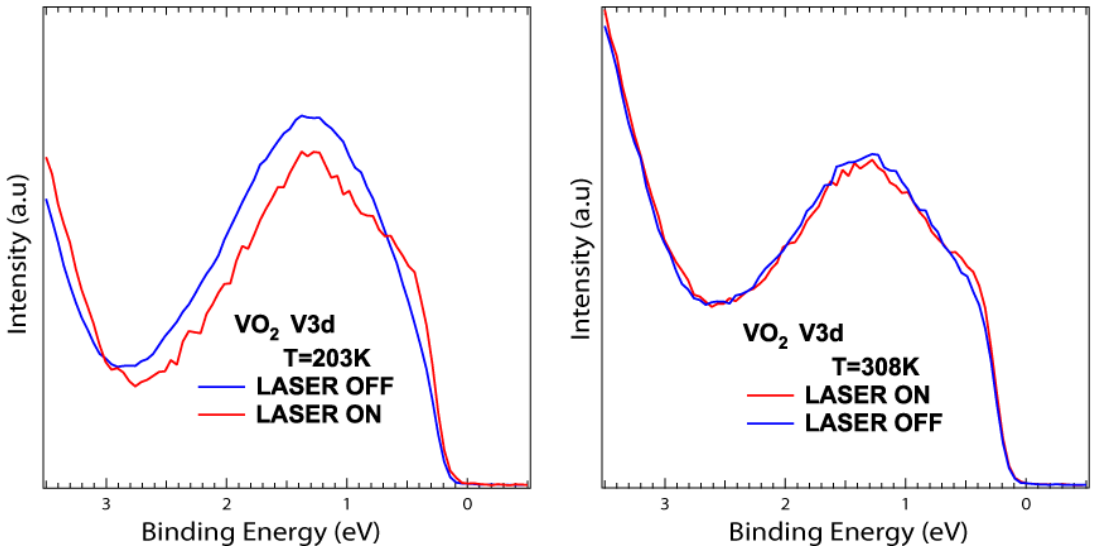

Figure 3.23: Valence band spectrum for 200 nm thick VO_2-film with and without laser excitation (3 μ J/Puls, 208.3 KHz repetition rate). a) Sample temperature T=203 K. b) Sample temperature T=308 K.

have been recorded, going from low to high temperatures and back to low temperatures. Figure 3.21b reveals that the most interesting amplitude to analyze is component 5, because it reflects the V 3d states close to the Fermi level. Figure 3.22 shows the amplitude A_5 as a function of the temperature. Changes are reversible and we observe a hysteresis width of 72 K.

3.2.3 Laser Excitation

In the VO_2 phase-transition changes of the electronic band structure are associated with atomic rearrangements between a low temperature monoclinic structure and a high temperature rutile phase. The intriguing nature of this process and the importance of phase transitions in metal oxides in modern condensed matter physics, makes this system interesting for ultrafast techniques. Several studies of ultrafast solid-solid phase transitions and the combined measurement of electronic and structural dynamics have been performed [Cav01, Cav94]. Such experiments raise several questions for future studies including the problems which microscopic process is responsible for initiating the structural distortion and what causes the disappearance of the band gap after optical excitation.

At a final step the phase transition was induced using a laser-pump synchrotron-probe measuring scheme. The amplified Ti:Sapphire laser delivers pulses with an energy of 6 μJ at 800 nm. The synchrotron was operating in multi-bunch mode.

Figure 3.23 shows photoelectron spectra of the VO_2 valence band for sample temperatures of 203 K and 300 K with and without laser excitation. After laser excita-

tion, the V3d-band shows the characteristic transformation to the rutile structure. Time-dependent studies after excitation reveal that the change at the V 3d edge is caused by heat accumulation and that changes within one laser period are in contrast insignificant. Thermal energy is at first concentrated at the VO_2 surface. By conduction, the heat is then transported to the bulk (SiO_2), which has a low heat conductivity. Therefore, the temperature of the sample raises and finally the phase transition takes place.